A Novel Dual-Patch Anti-Jam GPS Antenna

Frank N. Bauregger, Todd Walter, Dennis Akos, and Per Enge,
Department of Aeronautics and Astronautics, Stanford University

Biography

Frank N. Bauregger is a Ph.D. candidate in the Electrical Engineering Department at Stanford University. He received his B.S. in Electrical Engineering from the Pennsylvania State University. His research focuses on the design of interference resistant antennas for airborne GPS applications.

Todd Walter, Ph.D, is a research associate in the Department of Aeronautics and Astronautics at Stanford University. Dr. Walter received his Ph.D. in 1993 from Stanford and is currently developing WAAS integrity algorithms and analyzing the availability of the WAAS signal.

Dennis Akos completed his Ph.D. degrere in electrical engineering at Ohio University while conducting his graduate research within the Avionics Engineering Center. After completing his graduation he served as a faculty member with Luleå Techincal University, Sweden, and is currently a research associate with the GPS Laboratory at Stanford University. His research interests include GPS/CDMA receiver architectures, RF design, and software radios.

Per Enge, Ph.D., is professor of Aeronautics and Astronautics at Stanford University. A Ph.D. graduate of the University of Illinois, his research focuses on WAAS and LAAS aircraft landing applications.

Abstract

Antennas for airborne GPS applications would ideally have a radiation pattern which is uniform for elevation angles greater than 5°, and which has zero gain for angles below. Such an antenna would be immune to radio frequency interference (RFI) originating from below the aircraft, but would still provide coverage for low elevation GPS satellites. The popular microstrip patch antenna has a broad radiation pattern and typically allows reception of signals from all visible GPS satellites. However, as normally implemented, the microstrip patch is susceptible to RFI from below the aircraft.

This paper describes a novel dual-patch anti-jam GPS antenna which employs two independent microstrip patch antennas in a single package. The antenna is simple, inexpensive, and does not require external hardware or software for adaptive control. A nominal wide-looking patch is selected for GPS navigation when no interference is present. If GPS navigation is threatened by a jammer, the user may switch to an RFI resistant patch antenna. This is a half-wavelength nearly-square patch which has high gain toward the zenith and low gain toward the horizon. It will enhance high elevation satellites, but reject interference from the horizon or below the aircraft. Since this patch cannot acquire and track satellites below 10° elevation, the nominal patch should be used when no interference is present. Switching between the two antennas may be performed manually, or automatically by a smart GPS receiver which can detect the presence of RFI.

Switching between the two antennas is accomplished by means of properly biasing PIN diodes located beneath the patch elements. The PIN diodes are used to deactivate the patch which is not being used, while remaining transparent to the active patch. The dual-patch antenna is analyzed with a modified cavity model which accounts for the presence of the PIN diodes under the patch. Mutual coupling between the patch elements is also computed. The improved model provides the input impedance and radiation patterns for the patch.

A prototype dual-patch antenna has been built and tested. The transfer characteristic of the built-in low noise amplifier and band-pass filter was measured. In addition, rooftop testing of the prototype antenna demonstrated an RFI rejection performance improvement of 5 dB compared to a conventional patch antenna.

1. Introduction

The recent growth of wireless communication services and the impending implementation of ultra-wideband (UWB) data systems have heightened the concern for unintentional interference to GPS for airborne users.

Intentional jamming by hostile parties poses an additional threat to the availability of GPS for airborne navigation. These concerns warrant the development of a specialized interference resistant antenna which ideally has a uniform radiation pattern for elevation angles greater than 5°, and no response below. Toward that end, this paper describes a novel dual-element anti-jam GPS antenna. This antenna is simple in concept, inexpensive, and does not require external hardware or software typically required for an adaptive array antenna. In addition, this antenna is only slightly larger than conventional patch antennas found on aircraft today. Thus, it will directly replace a previously installed GPS patch antenna.

The dual-patch antenna has a nominal wide-looking element which is selected for GPS navigation when no interference is present. This antenna acquires and tracks GPS satellites down to the horizon. If GPS navigation is threatened by a jammer, the user may switch to an RFI resistant patch antenna. This is a half-wavelength nearly-square patch which has high gain (9 dBic) toward the zenith and low gain (-15 dBic) toward the horizon. This patch enhances high elevation satellites while rejecting interference from the horizon and from below the aircraft. Since the RFI resistant patch cannot acquire and track satellites below 10° elevation, it should not generally be used when no RFI is present. The nominal patch should be used is this case. Switching between the two antennas may be performed manually, or automatically by a smart GPS receiver which can detect the presence of RFI. Switching between the two antenna elements is accomplished by varying the DC voltage on the center conductor of the coaxial cable feedline connecting the antenna to the GPS receiver.

Analysis of the dual-patch antenna is performed by means of an improved cavity model. The conventional cavity model is modified to account for the presence of lumped loads beneath the patch. This is necessary to accurately model the effect of the PIN diodes which are located under both antenna elements. As with the traditional cavity model, input impedance and radiation patterns may be computed given the field distribution around the perimeter of the patch element. Mutual coupling is also included in the improved cavity model. This allows one to evaluate the degree to which the antenna elements may be operated independently from each other. It has been shown that the mutual coupling between two stacked patches is negligible (-25 dB) if one of the antennas is deactivated with forward biased PIN diodes. The improved cavity model is used to place the PIN diodes in favorable locations under the patch elements to achieve this effect.

A prototype dual-patch antenna was constructed and tested. The built-in low noise amplifier (LNA) and band-pass filter (BPF) provide 22 dB gain at L1, while significantly rejecting out-of-band signals. The noise figure of the antenna is estimated to be 2.6 dB.

2. Description of Antenna

A photograph of the prototype anti-jam GPS antenna is shown in Fig. 1. An aluminum ground plane supports the brass lower patch element, which is the RFI resistant antenna. The upper patch (copper) is the wide-looking nominal patch, and is stacked on the lower patch. Figs. 2 and 3 show a 3-D perspective and a vertical profile of the antenna, respectively.

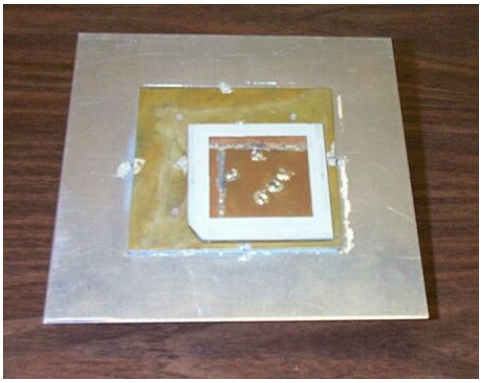

Figure 1: Photograph of dual-patch antenna.

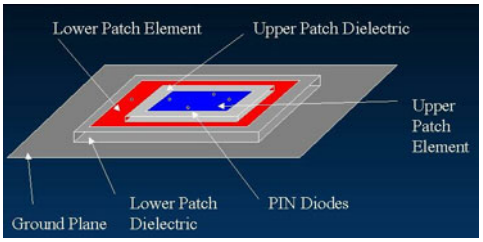

Figure 2: Three-dimensional view of dual-patch antenna.

The locations of the PIN diodes are indicated in these views. Both patches use a common feed which extends from the top patch through the bottom of the ground plane. The dielectric for the lower patch is Rohacell 51, which has a relative permittivity (ϵ_r) of 1.07. This low ϵ_r allows the dimensions of the lower patch to extend to nearly $\lambda/2$. Because of the shortening effect of the fringing fields around the perimeter of the patch, the dimensions are always less than $\lambda/2$.

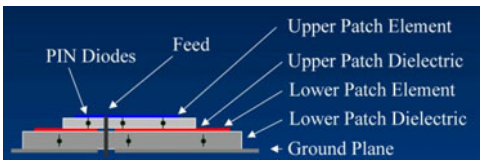

Figure 3: Vertical profile of dual-patch antenna.

This dielectric is 2 mm thick. The dielectric used for the upper patch is a 0.060 inch Rogers TMM 4 ceramic substrate, which is inexpensive and suitable for patch antennas because of its low loss. The ϵ_r is 4.50. The metals used for the final antenna will be copper, since it has superior electrical properties over brass and aluminum which were used in the prototype. The underside of the antenna is shown in Fig. 4. A cus-

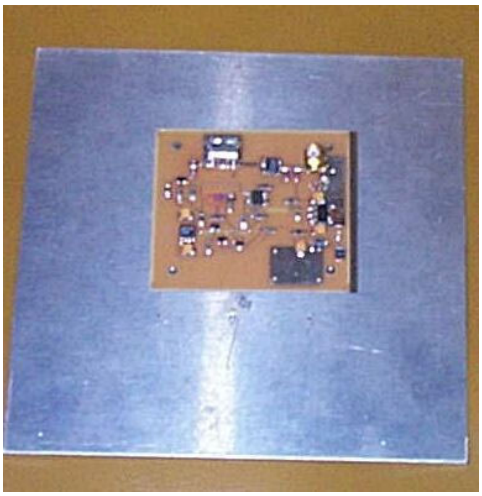

Figure 4: Photograph of dual-patch antenna RF and switching circuitry.

tom printed circuit board is shown which contains the LNA, BPF, and switching circuitry.

The only connection to the antenna is the coaxial RF feedline, which carries a DC voltage that serves to power the LNA and to switch between the two patch antennas. A system level block diagram is shown in Fig. 5. A control voltage of +5 volts DC powers the LNA, and selects the wide-looking patch. This means that the dual-patch antenna can replace nearly any active antenna on the market and function as a conventional patch antenna, remaining transparent to the user. If the control voltage is raised to +10 volts DC, the RFI resistant patch antenna is selected. The LNA remains powered on in this state, of course. The bias tee shown in Fig. 5 provides for manual control

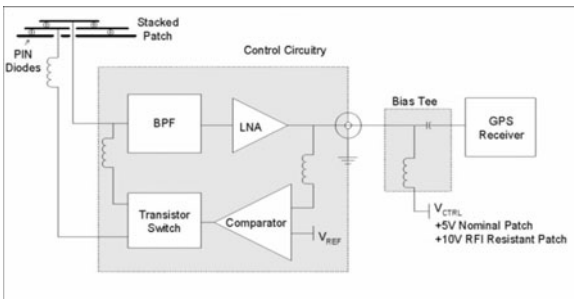

Figure 5: Block diagram of dual-patch antenna.

of the antenna. However, a pilot would likely desire a fully automated system whereby a smart GPS receiver decides that RFI is present, and switches to the RFI resistant patch. This level of sophistication may be achieved fairly easily by a simple firmware change in the GPS receiver, and a minor power supply modification.

3. Modeling the Dual-Element Antenna

The dual-element anti-jam antenna is modeled with an improved cavity model. The model incorporates the effects of the PIN diodes under the patch, as well as the mutual coupling between the upper and lower patches. The field distribution obtained from the improved cavity model gives the input impedance and also yields antenna radiation patterns.

Before introducing the improved cavity model, we first discuss the modeling of the PIN diodes which are placed underneath both patch elements. These PIN diodes act as lumped complex loads which draw current and modify the field distribution under the patch. An equivalent circuit model for the PIN diode is obtained from the datasheet. Consider a PIN diode which is reverse biased. In this state, the diode is nonconducting, and there is a separation of charges in the intrinsic (I) region of the device. The reverse biased PIN diode appears capacitive, with a small amount of series lead inductance. The equivalent impedance is on the order of $-j1000\Omega$ at L1. In a 50Ω circuit, this is nearly an open circuit, and will have very little effect on the antenna, except to shift the resonant frequency downward slightly. This effect can be reversed by simply designing the patch for a higher frequency (approximately 2 MHz at L1) than the desired operating frequency. When forward biased, the PIN diode turns on and becomes resistive, with a small amount of series lead inductance. The equivalent impedance is approximately $6 + j10\Omega$. This is a low impedance

relative to a 50Ω characteristic impedance, and will effectively short out the patch. These impedances for forward and reverse biased PIN diodes will be used as inputs to the improved cavity model.

The cavity model is a well known method for predicting the performance of microstrip patch antennas [1]. It is very simple and fast, and can provide results which are accurate to about 2.0%. The basic premise is that the field distribution under the patch can be expressed as a sum of weighted orthogonal basis functions, much like the Fourier series representation of a periodic signal. For a rectangular patch of width a, length b, and having a dielectric with thickness t and relative permittivity ϵ_r, Eq. 1 gives this field distribution. I_0 is the complex amplitude of the driving current source, which is located at (x_0, y_0).

$$V(x,y) = I_0(x_0,y_0) \cdot \left[-jtk \sum_{m=0}^{\infty} \sum_{n=0}^{\infty} \frac{\Psi_{mn}(x,y)\Psi_{mn}(x_0,y_0)}{k^2 - k_{mn}^2} \right] \quad (1)$$

For the rectangular geometry, the basis functions are sinusoidal, as given in Eq. 2.

$$\begin{aligned} \Psi_{mn}(x,y) &= \frac{\chi_{mn}}{\sqrt{ab}} \cos k_n x \cos k_m y, \text{ where} \quad (2) \\ k_n &= \frac{n\pi}{a}, \text{ and } k_m = \frac{m\pi}{b} \\ k_{mn}^2 &= k_m^2 + k_n^2 \end{aligned}$$

In Eq. 2, χ_{mn} is a normalizing constant [1], $k = \omega\sqrt{\mu\epsilon}$, and $Z_0 = \sqrt{\mu/\epsilon}$. This simple model does not account for the presence of lumped impedances underneath the patch.

In order to model this effect, we replace the lumped impedance with a current source having complex amplitude I_{PIN} [2]. The complex amplitude of the current source is determined by enforcing the boundary condition that the voltage appearing at the location of the current source is equal to $-Z_{PIN}/I_{PIN}$, where Z_{PIN} is the equivalent impedance of the PIN diode. The cavity model is then used to compute the required values of I_{PIN}, yielding Eq. 3.

$$I_{PIN} = -\{K_{PIN|PIN} + Diag[Z_{PIN}]\}^{-1} K_{PIN|(x_0,y_0)} \quad (3)$$

In Eq. 3, $K_{(x_1,y_1)|(x_2,y_2)}$ is the voltage at location (x_1, y_1) due to a current source at location (x_2, y_2), as given by the bracketed quantity in Eq. 1. The locations of the PIN diodes are denoted by PIN. The variables in Eq. 3 are matrices or columns of dimension $(n \times n)$ or $(n \times 1)$, respectively, where n is the number of PIN diodes beneath the patch. Z_{PIN} is a column vector containing the equivalent impedances of the PIN diodes. Now that the equivalent current sources have been solved for, we repeat the cavity model computation for the patch in Eq. 1, using the driving current I_0 and the equivalent PIN diode currents I_{PIN} as the sources. It is as if the patch were being excited by $n + 1$ current sources. The Equivalence Principle [3] is used to compute far field radiation patterns using the electric field distribution around the perimeter of the patch. In accordance with the assumed perfect magnetic conductor boundary condition on the perimeter, the magnetic field is zero at this location. This allows one to compute the radiation pattern of the antenna with knowledge of only the electric field around the perimeter. The input impedance to the patch is simply $-V(x_0, y_0)/I_0(x_0, y_0)$.

4. Analysis Results

The main purpose of modifying the cavity model as outlined in Section 3 is to account for the effects of the PIN diodes beneath the patch. We need this modeling technique to ensure that when forward biased, the diodes deactivate the undesired antenna, while when reverse biased, the diodes activate the desired patch. In addition, the cavity model will provide radiation patterns and the input impedance of the patch. The input impedance to both patches can be adjusted to $50 + j33\Omega$ by moving the feedpoint. The inductive component can be tuned out with a 3.3 pF chip capacitor. A mutual impedance calculation shows that there is only -25 dB of coupling between the two patches when one of them is deactivated. Therefore, the inactive patch will have essentially no effect on the radiation pattern of the active patch. In Fig. 6, we show an elevation plot of the dual-patch antenna mounted on a Cessna Caravan. A 10 dB improvement in RFI rejection is shown for jammers located at or below the horizon. In addition, the RFI resistant patch has approximately 3 dB more gain toward the zenith than the nominal patch. This will further serve to enhance reception of high-elevation GPS satellite signals, while rejecting ground-based RFI. In Fig. 7 we show the roll plane radiation pattern of the dual-patch antenna. The same RFI rejection performance is anticipated in the roll plane as that observed in the elevation plane. One striking feature in Fig. 7 is the effect of diffraction around the wings which creates deep nulls below the aircraft in this plane.

Commercial and private pilots desire an anti-jam GPS antenna which will also receive WAAS broadcasts. Users in CONUS currently receive WAAS messages from two geosynchronous satellites, which also provide GPS-like ranging signals. WAAS availabil-

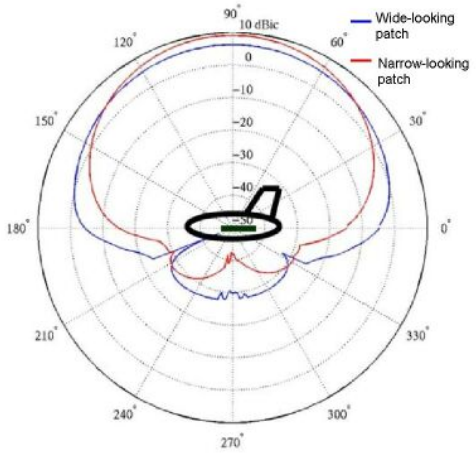

Figure 6: Elevation radiation pattern of dual-patch antenna on Cessna Caravan.

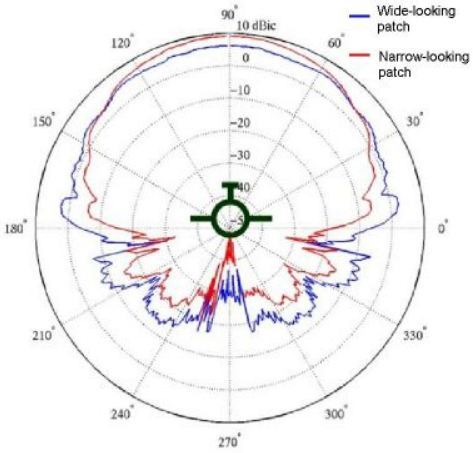

Figure 7: Roll plane radiation pattern of dual-patch antenna on Cessna Caravan.

ity is targeted at 99.9% for users in CONUS, with no RFI. However, a strong interference source can reduce availability to 0% when using a standard microstrip patch antenna. In Fig. 8 we show the availability of WAAS for users in CONUS experiencing this level of interference, but using the interference resistant patch antenna instead of a standard patch. Here we assume the level of RFI is sufficient to completely jam the standard patch antenna, reducing WAAS availability to 0%. Our antenna will provide 1 NM horizontal navigation 50% of the time over 50% of CONUS. While this is not very impressive, the alternative is to have no GPS navigation capability using a standard patch. The 1 NM HAL was chosen since it represents the required navigation performance (RNP) to execute a missed approach procedure [4]. It is assumed that the pilot will begin this maneuver when RFI is detected and GPS navigation is threatened.

If an additional geosynchronous satellite is placed at 120°W, and the aircraft is able to use the barometric altimeter to aid the navigation solution, WAAS availability improves significantly. In Fig. 9, we observe that with aiding, WAAS is available to 75% of CONUS at least 75% of the time. In addition, we have tightened the alarm limits in Fig. 9 to meet the general WAAS LNAV/VNAV criteria. So even in a fully jammed state, horizontal and vertical guidance are available to the pilot using the RFI resistant patch with aiding.

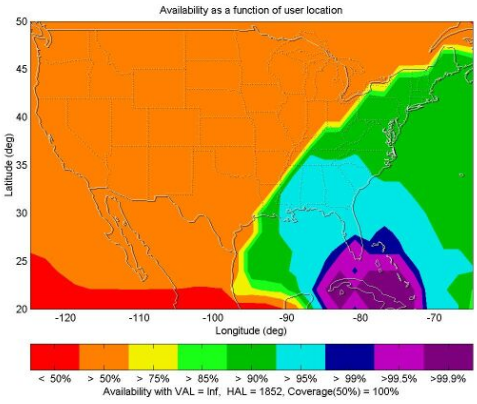

Figure 8: WAAS availability with RFI using current GPS constellation and RFI resistant patch.

5. Experimental Results

A prototype dual-patch antenna has been built and tested. The LNA/BPF combination was characterized by measuring S_{21} with a network analyzer. In Fig. 10, we see that the circuit has 22 dB gain at L1, while achieving significant attenuation of out-of-band signals. For example, signals in the 900 MHz cellular band are 70 dB down from the response at L1. Using nominal specifications from the datasheets, the estimated noise figure of this antenna is 2.6 dB. In the next experiment, the antenna was placed on the roof of the lab and connected to a GPS receiver. A broadband noise source located below the antenna in the lab was activated for 10 minute intervals. In Fig. 11 we show the C/N_0 of one GPS satellite over a 30

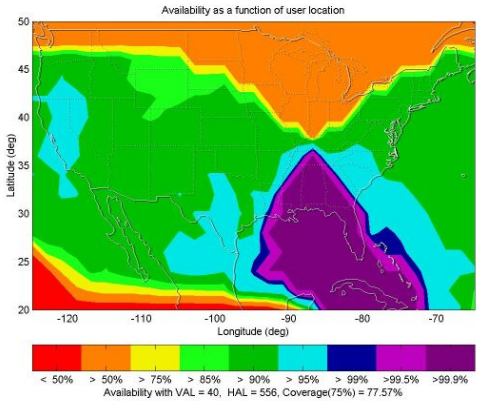

Figure 9: WAAS availability with RFI using barometric altimeter aiding, additional geosynchronous satellite at 120°W, and RFI resistant patch.

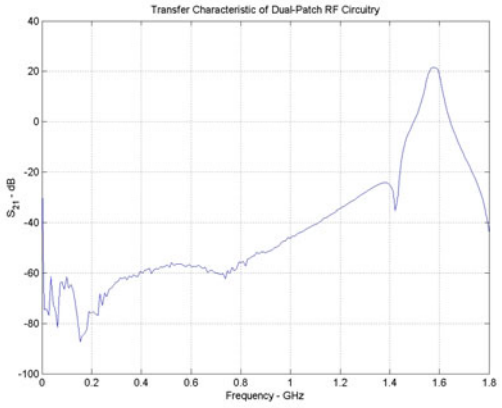

Figure 10: Measured response of LNA/BPF combination.

minute period. The satellite reached an elevation angle of 70°. The nominal patch with no jamming tracks the satellite at about 50 dB C/N_0 throughout this run. When the jammer is activated, the C/N_0 drops to 45 dB. The RFI resistant patch tracks the satellite at 52 dB C/N_0, confirming the expected higher zenith gain. When the jammer is activated, the C/N_0 only drops to 49.5 dB using the RFI resistant patch. We conclude from this simple experiment that the RFI resistant patch provides a net 4.5 dB advantage over the nominal patch in this case. This particular satellite yielded the worst case results; data from all other satellites show a net $5-6$ dB advantage. More careful design of the dual-patch antenna should yield even better performance. It is hoped that the final design will show a net 10 dB improvement.

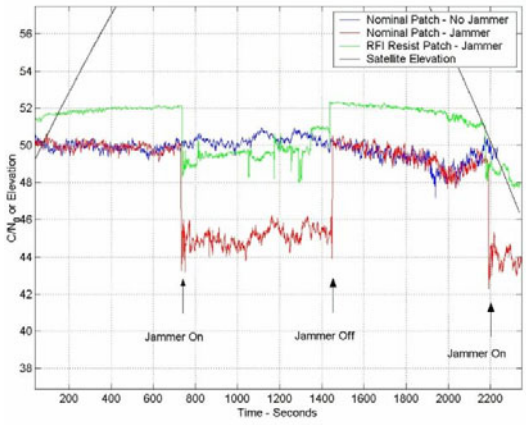

Figure 11: Tracking one GPS satellite with and without jammer.

6. Conclusions

This paper described the design, analysis, and prototype testing of a novel dual-element anti-jam GPS antenna. The antenna makes use of two microstrip patch antenna elements which can operate independently of each other. A nominal patch provides a broad radiation pattern for GPS navigation when no RFI is present. The user can switch manually or automatically to an RFI resistant patch when RFI is detected. The RFI resistant patch cannot track satellites below 10° elevation, so the nominal patch should be selected for general use when no RFI is present. The antenna is small, lightweight, inexpensive, and requires no additional external hardware or software to operate. It is a direct replacement for nearly any conventional aviation microstrip patch antenna found on the market today. The antenna provides a 5 dB increase in RFI rejection over a conventional patch antenna. It is hoped that future improvements to the antenna will yield a net 10 dB improvement.

7. Acknowledgments

The authors would like to acknowledge the FAA Satellite Navigation Product Team for sponsoring the research reported in this paper. The authors also wish to thank Dr. Sam Pullen for the use of Stanford LAAS Lab resources during the design and test phases of this project, and Aldo Rossi, who provided invaluable advice in the area of machining and metal work. The authors also acknowledge the generosity of the Metelics Corporation for providing engineering samples of their PIN diodes.

References

[1] K. R. Carver and J. W. Mink. Microstrip Antenna Technology. *IEEE Transactions on Antennas and Propagation*, AP-29(1):2 – 24, January 1981.

[2] S. Mutlu and M. I. Aksun. Hybrid Model for Probe-Fed Rectangular Microstrip Antennas With Shorting Pins. *IEEE Antennas and Propagation Society International Symposium*, 3:1448 – 1451, 2000.

[3] C. A. Balanis. *Advanced Engineering Electromagnetics*. Wiley, New York, New York, 1989.

[4] DOT/FAA. *Order 8260.48: Area Navigation (RNAV) Approach Construction Criteria*. April 8, 1999.